Parkinson's protein α-synuclein : membrane interactions and fibril structure

Kumar, P.

5 Nanometer Distance Constraints for the Fold of α-Synuclein in Fibrils of Single Morphology

5.1 Introduction

After Alzheimer's disease, Parkinson's disease (PD) (1) is the most highly spread neurodegenerative disease. This disease is characterized by the presence of intracellular protein inclusions, called Lewy bodies (2,3), in the brain of PD patients. Lewy bodies are largely composed of α-Synuclein (αS) (4,5). The protein αS, which has a physiological function that is yet unknown, is 140 amino-acids long. It is an intrinsically disordered protein (6,7), which under certain conditions can form fibrils.

Amyloid fibrils have a cross β-sheet structure (8) shown schematically in Figure 5.1. In the fibril, each protein has a well-defined conformation. The protein is arranged into several consecutive β-strands that are connected by turns, as shown in Figure 5.1a. These individual β-strands, which run perpendicular to the fibril axis, combine to β-sheets, which are shown as colored planes in Figure 5.1b. The β-sheets grow in the direction of the fibril axis. The architecture of fibrils is more complex. Longer peptides, such as αS can form multiple β-sheets and pairs of β-sheets can be at an angle to each other (9). Therefore, the fold of a protein such as αS in the fibril is a challenging question. It is important to understand which residues are involved in the fibrillization and to identify interactions that hold the fibril together.

Solid-state nuclear magnetic resonance (ss-NMR) (10) and electron paramagnetic resonance (EPR) studies (11,12) have identified residues that are present in the β-sheets. Not all ss-NMR studies agreed on the extent of β-sheets, and several (13,14) showed doubling of NMR signals interpreted as polymorphism of the fibrils, i.e., different fibril forms in one sample. Polymorphism can influence the internal structure of fibrils (15).

Several studies (16–24) were done on the αS fibril fold. Two studies (23,24) discuss the structure of αS in the fibril at atomic resolution, employing the non-amyloid-beta-component (NAC) region of αS. Recently, an ss-NMR study by Tuttle *et al*. (25) presented a model at atomic resolution of full-length αS in fibrils.
Along with the structural information obtained from NMR studies, distance constraints in the nanometer range can be of great help to define the fibril fold, as shown recently for islet amyloid polypeptide (IAPP) (26). To obtain such long-range distance constraints, a pulsed EPR method, double electron-electron resonance (DEER) (27–30), is attractive. It can measure distances between 2 and 5 nm. In this work, we use DEER to obtain distances in the nanometer range, i.e., the intramolecular distances between two spins, from the fibrils of doubly spin-labelled αS mutants.

To control the morphology of the fibrils, conditions are used that were optimized in (31) to obtain fibrils of single morphology. Fibril samples of all αS spin-labelled constructs are grown by seeded fibrillization. A single batch of wt-αS seeds, which was grown as described in (31) (see Materials and methods), is used for each sample. In chapter 4, we described the characterization of the fibril morphology by transmission electron microscopy (TEM) and discussed our findings in detail, demonstrating that we are able to control the morphology of fibrils to a reasonable extent.

Similar to previous approaches (17,18,21,22), intramolecular distances are measured on doubly spin-labelled αS. We prepared a set of nine double cysteine mutants and their respective single-cysteine references and labelled them with MTSL [(1-oxyl-2,2,5,5-tetramethylpyrroline-3-methyl)-methanethiosulfonate]. We refer to the doubly-labelled constructs as αS42/69, αS42/75, αS42/85, αS56/69, αS56/75, αS56/90, αS69/85, αS69/90, and αS75/85 where the numbers denote

the labelling position in the protein sequence. As before (22), diamagnetic dilution was used, generating fibrils composed of 95 % wt-αS in case of doubly labelled αS and 90 % for singly labelled αS.

We show that long–range distance constraints for the αS fibril fold can be obtained under conditions that promote fibrils of single morphology. We obtain nanometer distance constraints from eight doubly-labelled αS constructs by DEER from pairs of residues that span the entire β-sheet region of αS, from residue 42 to residue 90. We also compare our distances to distances obtained in previous DEER studies (18,21,22) and to two NMR studies (24,25) at atomic resolution of the αS fibril fold.

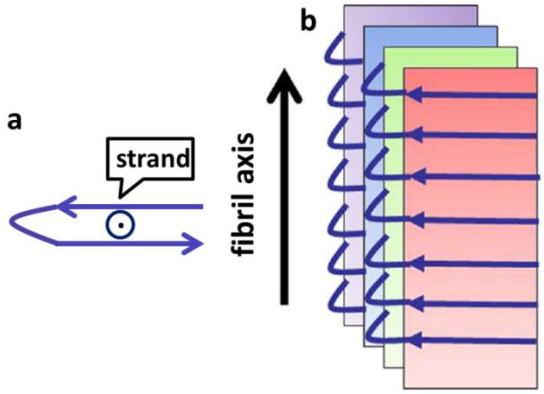

Figure 5.1. Schematic representation of the overall structure of amyloid fibrils. a: blue arrows represent a β-strand and the blue dot shows the direction of the fibril axis, which is pointing out of the page. b: the black arrow represents the direction of the fibril axis and colored planes depict the β-sheets. The Figure is modified from (22).

5.2 Materials and methods

5.2.1 Expression and purification of cysteine mutants of the α-Synuclein protein

Single and double cysteine mutations were introduced into the αS gene by site-directed mutagenesis. Mutants were expressed in the *Escherichia coli* strain BL21(DE3) and subsequently purified in the presence of 1 mM DTT (32,33). Prior to labelling, αS mutants were reduced with a sixfold molar excess (per cysteine) of DTT for 30 min at room temperature. Subsequently, samples were desalted on Pierce Zeba5 mL desalting columns, followed by an immediate addition of a sixfold molar excess (per cysteine) of the MTSL spin label[(1-oxyl-2,2,5,5-tetramethylpyrroline-3-methyl)-methanethiosulfonate]and incubated for 1 h in the dark at room temperature. Free label was removed using two additional desalting steps. Protein samples were applied onto Microcon YM-100 spin columns to remove any precipitated and/or oligomerized proteins and diluted into 10 mM Tris–HCl, pH 7.4 to typical protein concentrations of approximately 0.25 mM (34).

5.2.2 Preparation of αS fibril seeds

For seeds, we first prepared wild type (wt) αS fibrils following the protocol from Sidhu *et al*. (31), described briefly. The wt-αS protein solution (concentration = 100 µM, in 10 mM Tris-Cl buffer, pH 7.4, containing 10 mM NaCl and 0.1 mM EDTA) was aliquoted into 15 Eppendorf tubes (Eppendorf LoProtein Bind 2 ml), 500 µl each. All tubes were incubated at a temperature of 37 ^{o}C shaking continuously at 500 rpm in a Thermo mixer (Eppendorf). The time evolution of αS fibrillization was monitored by the standard Thioflavin T (ThioT) fluorescence assay. For each tube, fibrillization was stopped when the ThioT-fluorescence

intensity reached a plateau. The fibrillization was completed in 6-7 days. The content of each Eppendorf tube was divided into two samples of 250 µl each, which were frozen quickly in liquid nitrogen and stored at – 20 ^{o}C. To start the seeded fibrillization experiment, one aliquot was thawed and sonicated in a bath sonicator (Branson 2510) for one minute to break the fibrils into seeds, which were then added to the samples to be fibrillized.

5.2.3 Seeded fibrillization of spin labelled αS and harvesting

We prepared the fibrils by mixing the monomeric αS (spin-labelled and wild type αS) with the wt-αS seeds. The total monomer concentration used for making fibrils was 100 µM. To this mixture 2 % monomer-equivalent seeds were added.

Diamagnetic dilution was employed to diminish the effect of intermolecular interaction. We used 1:20 (SL αS:wt) diamagnetic dilution for all doubly labelled and 1:10 diamagnetic dilution for all singly labelled αS. A typical sample for doubly labelled αS consisted of 5 µM spin-labelled αS, 95 µM wt-αS and 2 µM αS-monomer equivalent seeds. The total volume for each sample was 3.0 ml, which was aliquoted into five Eppendorf tubes and put on the thermomixer. The seeded fibrillization was performed under the same conditions as used for wt-αS fibrils (31). The time evolution of seeded fibrillization was monitored by the ThioT fluorescence assay. Most of the mutants completed the aggregation in 24 hours except for αS69/90, which took 9 days. Seeded fibrils were harvested by ultra-centrifugation for 45 min at 120000xg using a 70.1Ti rotor in a Beckman Coulter Ultracentrifuge. The fibril pellets were washed three times with the buffer used for fibrillization. The washed pellets were used for making samples for DEER measurements.

The spin concentration of spin-labelled protein was determined by comparing the double integral of the room temperature, liquid solution EPR spectrum to that of

a reference sample of known spin concentration. The protein concentration and the labelling degree are given for each sample in Table 5.1. To compensate for incompletely spin-labelled protein, actual protein concentrations used to make samples were calculated based on the amount of spin label in each protein. In Table 5.1, also the diamagnetic dilution is given that would result if the protein had been completely labelled.

Table 5.1. Protein concentrations in the αS fibrillization solution and labelling degree of proteins

αS fibril sample	**labelling degree (%)[a]**	**concentration of spin-labelled protein (μM)[b]**	**concentration of wild type protein (μM)[b]**	**nominal diamagnetic dilution [SL αS : wt αS][c]**
αS42/69	55	9	91	1 : 11
αS42/75	48	10	90	1 : 10
αS42/85	62	8	92	1 : 12
αS56/69	73	7	93	1 : 14
αS56/75	56	9	91	1 : 11
αS56/90	55	9	91	1 : 11
αS69/85	82	6	94	1 : 17
αS69/90	85	6	94	1 : 17
αS75/85	60	8	92	1 : 12

a: Percentage relative to 100 % doubly spin-labelled protein. **b:** Protein concentration in the fibrillization solution. **c:** Diamagnetic dilution, if protein had been 100 % spin-labelled.

5.2.4 Transmission electron microscopy

Negative staining of the αS-fibril samples was done by placing a fresh carbon-coated grid (200 meshes) on top of a drop (10 μl) of the αS-fibril solution for 2 minutes. The grid was then washed 3 times on a drop of distilled water.

Subsequently, the grids were placed directly on top of a small drop of 3.5 % uranyl acetate for 1.5 minutes and the excess uranyl acetate was blotted away by touching the grids to a filter paper at an angle of 45°. Afterwards the grids were placed in a Petri dish with filter paper to let them dry. The grids were examined with a FEI Technai-12 G2 Spirit Biotwin transmission electron microscope (FEI, Eindhoven, Netherlands) and micrographs were taken with a Veleta side-mounted TEM camera using Radius acquisition software (both Olympus Soft Imaging Solutions, Münster, Germany). Images were measured using the image processing feature within the Radius software package.

5.2.5 Continuous-wave EPR at 120 K

The 9.7 GHz cw-EPR measurements were performed using an ELEXYS E680 spectrometer (Bruker, Rheinstetten, Germany) with a rectangular cavity, using a modulation frequency of 100 kHz. For measurements at 120 K, a helium gas flow cryostat (Oxford Instruments, United Kingdom) with an ITC502 temperature controller (Oxford Instruments, United Kingdom) was used. For the measurements in frozen solution, 3 mm outer diameter quartz sample tubes were used. To obtain a frozen glass 20 % glycerol was added to the samples before freezing them in liquid nitrogen. The frozen samples were inserted in the pre-cooled helium gas flow cryostat. The EPR spectra were recorded using a modulation amplitude of 0.2 mT and a microwave power of 0.16 mW. Typical accumulation times were approximately 70 min.

5.2.6 DEER measurements

All DEER experiments were done at 9.5 GHz on an ELEXSYS E680 spectrometer (Bruker, Rheinstetten, Germany) using a 3 mm split-ring resonator (ER 4118XMS-3-W1). We performed the measurements at 40 K with a helium-gas flow using a

CF935 cryostat (Oxford Instruments, United Kingdom). The pump and observer frequencies were separated by 70 MHz and adjusted as reported before (35). The pump-pulse power was adjusted to invert the echo maximally (27–30). The pump-pulse length was set to 16 ns. The pulse lengths of the observer channel were 16 and 32 ns for π/2- and π - pulses, respectively. A phase cycle (+ x) - (- x) was applied to the first observer pulse. The complete pulse sequence is given by $\frac{\pi}{2}_{\mathrm{obs}} - \tau_1 - \pi_{\mathrm{obs}} - t - \pi_{\mathrm{pump}} - (\tau_1 + \tau_2 - t) - \pi_{\mathrm{obs}} - \tau_2 - \mathrm{echo}$. The DEER time traces for ten different values of τ_1 spaced by 8 ns starting at τ_1=200 ns were added to suppress proton modulations. Typical accumulation times per sample were 14 - 17 hours.

5.2.6.1 DEER analysis

In order to analyze the DEER traces and extract the distance distributions, the software package “DeerAnalysis 2011” was used (36). Experimental background functions were derived from DEER traces of singly labelled αS under conditions of diamagnetic dilution. The distance distribution was derived by the model free Tikhonov regularization (27–30,36). The width of the peaks were determined by fitting each individual peak of the distance distribution curve obtained from the DEER analysis using a Gaussian fit function provided in Origin non-linear curve fitting tools (Origin Pro 9).

5.2.7 MMM analysis

To compare the distances obtained in the present study with recently reported models of the αS fibrils (25) and their core (24), we used the multiscale modeling of macromolecular systems (MMM) software (MMM version 2013)(37). It enables

to model the spin-label linker conformation at the desired positions of the protein to determine the distance distribution for each pair of spin-labels.

5.3 Results

The details of the results of the morphology of fibrils are described in chapter 4 of this thesis. Figure 5.2 shows TEM images of the fibrils grown for the present study. All fibrils were prepared using one batch of seeds and conditions described in Materials and methods. Single fibrils have a width of 5.6 ± 1 nm (Figure 5.2f, black arrows) and are often found to twin with another fibril that runs parallel to generate a width of 9 -10 nm (see Figure 5.2a, black arrows). Many of these twinned fibrils are twisted, as indicated in Figures 2c and 2f by white arrows, showing a periodicity around 170 nm, 240 nm, and 290 nm.

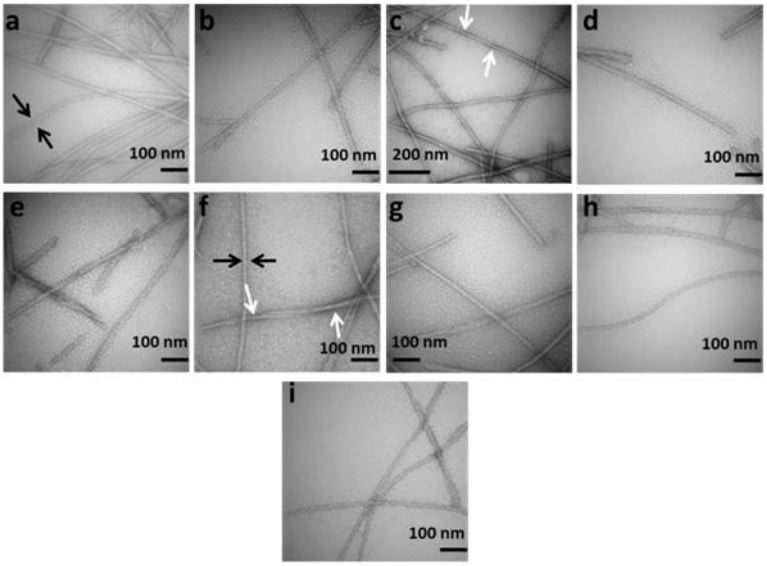

Figure 5.2. Morphological characterization of αS fibrils used in this study: Negative stain transmission electron microscopy (TEM) images of a. αS42/69, b. αS42/75, c. αS42/85, d. αS56/69, e. αS56/75, f. αS56/90, g. αS69/85, h. αS75/85, and i. αS69/90. Black arrows indicate the width of the twinned fibril (a) and of the single fibril (f), while the white arrows at a twist show the points between which the periodicity of twists was measured.

5.3.1 DEER results

In Figure 5.3a, the DEER time traces of fibrils grown from the doubly spin-labelled proteins are shown. The traces look different. Almost all DEER traces have a slow initial decay showing the absence of short distances. In Figure 5.3b the DEER time traces of αS56/69 and αS56/90 fibrils fibrillized under conditions employed in the present study (for details, see Materials and methods) are compared to those described by Hashemi Shabestari *et al.*(22). For clarity, from now on, we use the nomenclature ***αS56/69*** and ***αS56/90*** for αS56/69 and αS56/90 fibrils described in Hashemi Shabestari *et al.*(22). The DEER trace of ***αS56/69*** (22) shows a fast initial decay, which is absent in the trace of αS56/69 fibrils. Also the respective traces of the fibrils from αS56/90 differ. The trace of ***αS56/90*** has a fast decay component that is absent in the trace of αS56/90 fibrils.

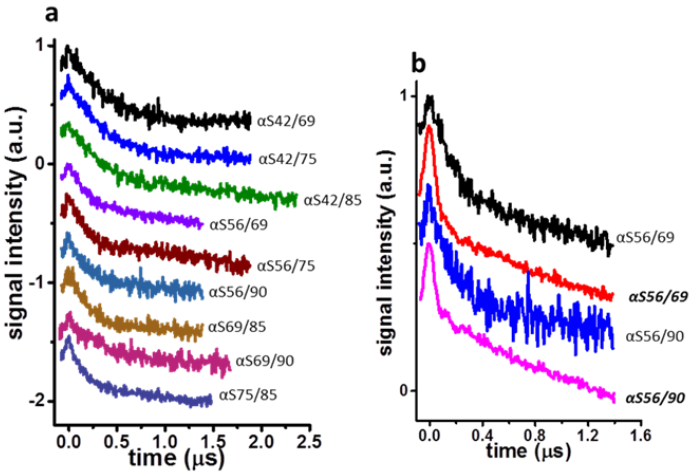

Figure 5.3. DEER time traces of αS fibril samples: a. αS fibril samples grown under seeded conditions, b. comparison of DEER time trace of αS56/69 with ***αS56/69*** and αS56/90 with ***αS56/90***. ***αS56/69*** and ***αS56/90*** stand for fibrils of αS56/69 and αS56/90 respectively grown under conditions described by Hashemi Shabestari *et al*.(22). All traces are normalized, i.e., the maximum echo intensity is set to one and the traces are shifted vertically for better visibility.

In Figure 5.4, the steps of the analysis of DEER traces are shown. Figure 5.4a shows the DEER traces along with the background trace derived from a 1:1 addition of the DEER curves of the respective singly labelled αS variants. Figure 5.4b shows the background-corrected data and the fits corresponding to the distance distributions shown in Figure 5.4c, d, and e. The modulation depths and the parameters of the distance distributions are given in Table 5.2. For most of the αS mutants the modulation depth is 0.3 to 0.5, showing that the majority of the spin labels in the sample are involved in a two-spin interaction.

Fibrils of αS69/90 have DEER traces with a comparatively low modulation depth, i.e., around 0.2. This low modulation depth shows that the number of coupled spins contributing to the distance distribution is low, which indicates that a significant population of the protein has a conformation with distances outside the DEER measurement range, i.e., distances shorter than 2 nm or longer than 5 nm. Therefore, we did not process the DEER data of the αS69/90 fibril sample further. The distance distributions of the αS variants αS42/69, αS42/75, and αS56/69 show two peaks and the remaining ones have just one peak. Most of the peaks in the distance distributions have a width of approximately 0.8 nm (Table 5.2).

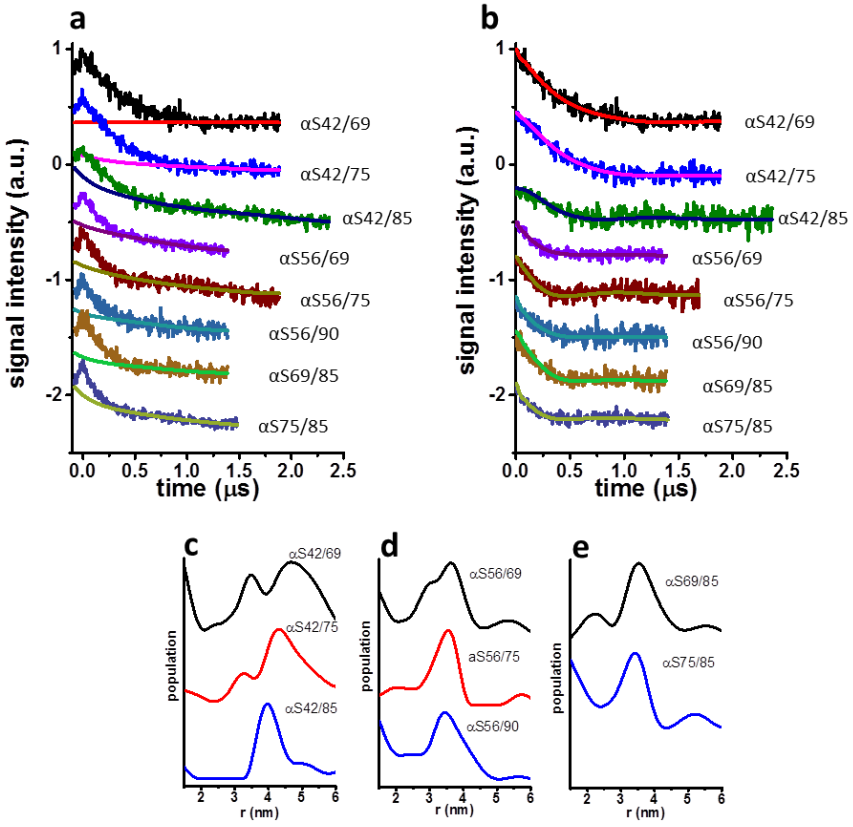

Figure 5.4.DEER analysis for αS fibril samples: a. DEER time traces with experimental background, b. DEER time traces after background correction along with the fits corresponding to the distance distributions shown in c, d, and e; c. for αS42/69 (black), αS42/75 (red) and αS42/85 (blue), d. for αS56/69 (black), αS56/75 (red) and αS56/90 (blue), and e. for αS69/85 (black), αS75/85 (blue); distance distributions were derived from the DEER data after Tikhonov regularization with regularization parameter α of 1000. The DEER data of the αS69/90 fibril sample is not included because of the low modulation depth (see Table 5.2). All traces are normalized (maximum echo intensity is one) and shifted vertically for better visibility.

Figure 5.5 shows the distance distributions of ***αS56/69*** and ***αS56/90*** fibril samples described in (22) in comparison with those of αS56/69 and αS56/90. In (22), intramolecular distances found were 2.1 nm (for ***αS56/69***) and 3.4 nm (***αS56/90)***.

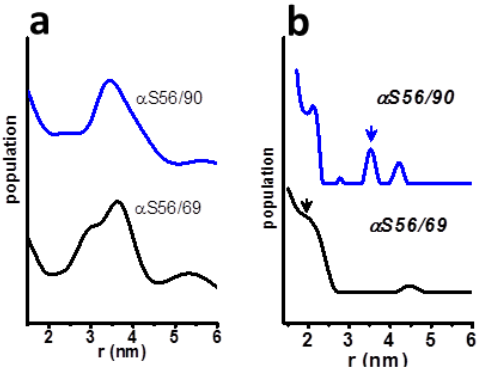

Figure 5.5. Comparison of distance distribution of fibrils of a) αS56/90, and αS56/69, grown under the conditions in the present study with b) ***αS56/90***, and ***αS56/69***, described in (22). Arrow depicts the intramolecular distances for b. For a, distances are shown in Table 5.2.

Table 5.2. Parameters of distance distributions of αS fibrils. FWHM: Full width at half maximum (for details, see Materials and methods). The modulation depth of the DEER trace is obtained from DEER analysis, the distances and the width from Gaussian fits to the individual peaks of the distance distribution (for details see Materials and methods)

αS variants	**modulation depth**	**distances (nm) and FWHM (nm) of peaks**				**cw-EPR line broadening** [a]
		peak 1	**FWHM**	**peak 2**	**FWHM**	
αS42/69	0.49	3.4	0.5	4.6	1.4	no
αS42/75	0.55	3.3	0.8	4.3	0.8	no
αS42/85	0.25	4.0	0.7	na	na	no
αS56/69	0.25	3.0	0.9	3.7	0.7 [b]	no
αS56/75	0.32	3.5	0.8	na	na	yes
αS56/90	0.33	3.5	1.1	na	na	yes
αS69/85	0.39	3.5	0.9	na	na	yes
αS75/85	0.29	3.4	0.8	na	na	no
αS69/90	0.21	modulation depth too low for meaningful distance distributions				no

na: not applicable; **a:** see appendix C; **b**. analysis with two peaks is probably not meaningful given the small separation and the large width, i.e., FWHM, of each peak.

5.3.2 MMM derived distance distributions

The experimentally measured distances are between the nitroxide groups of two spin labels. The spin-label linker, which separates the nitroxide from the protein backbone, is about 0.5 nm in length and also flexible. Therefore, the spin-label linker length and flexibility has to be taken into account to compare the distance measured by DEER to the fibril structure from crystallography or NMR studies. Spin-label linker conformations were calculated by the rotamer-library based method with the multiscale modeling of macromolecular systems (MMM) software (37). The experimental distance distributions were compared with the MMM simulations of the distance distributions based on the fibril structure published recently by Tuttle *et al*. (25) (PDB accession number: 2N0A).

Figure 5.6 shows the experimental DEER traces of all αS fibrils used in the present study and their corresponding distance distributions in comparison to those derived from MMM. To distance distributions derived from MMM, we refer as MMM distance distributions. All MMM distance distributions have narrower peaks than the experimental ones. For αS42/69 (a), αS42/75 (b), αS42/85 (c), αS56/69 (d), and αS56/75 (e), the MMM distance agrees with one of the experimentally observed distances, while for αS56/90 (f), αS69/85 (g), and αS75/85 (i), no such agreement can be seen. The short MMM distance for αS69/90suggests broadening of the cw-EPR spectra, which is not observed experimentally (see Table 5.2).

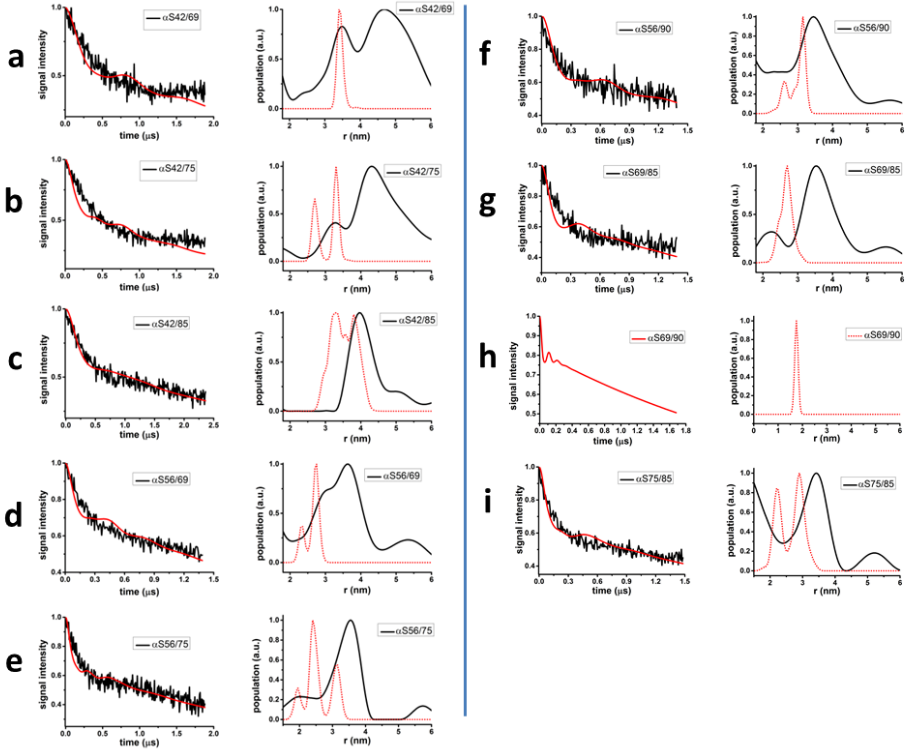

Figure 5.6. Comparison of DEER experimental data with those derived by simulation from the PDB structure of αS-fibril, which we refer to as the Rienstra model (25) (Accession no: 2N0A) using the MMM analysis package: Superposition of experimental DEER traces of αS fibrils and their distance distributions (both shown as a black line) with MMM DEER traces (red line) and their distance distributions (shown as a red dotted line) respectively derived from MMM analysis. a. αS42/69, b. αS42/75, c. αS42/85, d. αS56/69, e. αS56/75, f. αS56/90, g. αS69/85, h. αS69/90, and i. αS75/85.

5.4 Discussion

We have investigated fibrils of a set of SL-αS variants containing two spin labels, for which fibrils of SL-αS variants containing one spin label are also needed. Using seeded fibrillization with seeds derived from one batch of wild-type αS grown under the conditions optimized in (31), we avoid polymorphism as much as possible.

The detailed study of the morphology of fibrils is described in chapter 4 of this thesis. Transmission electron microscopy on all doubly labelled fibrils used in the present study shows similarity in their morphologies (see Figure 5.2). We observe differences in the periods of the twists, however, as described in chapter 4, the small number of observations and the difficulty in detecting the cross-over points makes it difficult to determine period lengths accurately. The remaining parameters show that the fibril morphology is similar for all constructs, assuring that distances from all constructs relate to one fibril-morphology.

5.4.1 Distances from DEER experiments

Distances are obtained between eight pairs of residues, which cover the entire fibril core of αS. The distances are listed in Table 5.2, from which we discuss a few peculiarities. One is the αS69/90 mutant that has a low modulation depth, which indicates distances outside the sensitivity range of DEER. We exclude short distances because of the absence of line broadening in cw-EPR spectra (see appendix C) and therefore conclude that the distance between residue 69 and 90 is larger than 4 nm.

The distance distributions of αS42/69 and αS42/75 (Figure 5.4c, top two traces) show two distances, although, under normal circumstances, only one distance is expected. Intermolecular distances, i.e., distances between spin labels at different proteins in the fibril could be a source of additional distances. Intermolecular interactions would also increase the modulation depth, which is relatively high for αS42/69, and αS42/75. Intermolecular interactions could be stronger for αS42/69, αS42/75, αS56/75, and αS56/90 because the degree of spin-labelling of the starting protein was low in these samples. The low degree of labelling was compensated for by adding relatively more spin-labelled protein to the sample

(see Materials and methods, and Table 5.1). If the degree of labelling is low because both spin-label positions are incompletely labelled to the same degree, for example label position 1, 50 % and position 2, 50 %, no complication arises, but if the spin-labelled protein contains a substantial amount of protein that is only singly labelled, a lower contribution of intramolecular distances results, giving a larger contribution of intermolecular versus intramolecular interactions. Therefore, one of the two distance peaks observed in DEER for αS42/69 and αS42/75 might be due to intermolecular interactions. For the αS56/75 and the αS56/90 mutants, we attribute the short distance component observed by broadening of the cw-EPR spectra (see appendix C) to intermolecular interactions. Additional experiments, starting with protein of higher degree of labelling, and fibrils prepared with higher diamagnetic dilution would be needed to decide which of the distances in the distributions of these mutants are inter or intramolecular.

While annoying, the setup of the present study made it impossible to avoid these complications. The ultimate goal, to use these long-range constraints to build and test atomic models of the fibril fold, requires a large number of double mutants, fibrillized under single morphology conditions, making it impossible to optimize every single set of double-mutant DEER measurements. In the analysis so far and for future model building, we take into account that some distances can be intermolecular. Obviously, atomic models can also find inconsistencies in the distances, which arise from the experimental limitations. Therefore, we expect to refine the interpretation in the future.

5.4.2 Comparison with DEER distances from other studies

Previously, in our lab, we performed DEER experiments on αS fibrils (22). These fibrils were grown under different conditions than used in the present study. The distances are compared in Table 5.3.

Table 5.3. Comparison of αS fibril distances from the present study with those from Hashemi Shabestari *et al*. (22)

spin-label positions	**distances (nm) from the present study**		**distances (nm) (22)**
	peak 1	**peak 2**	
αS56/69	3.0	3.7	2.1 nm
αS56/90	3.5		3.4 nm
αS69/90	> 4.0 nm		> 4.0 nm

For the αS56/69 mutant, the distances differ. For ***αS56/69,*** the distance of 2.1 nm dominates (Figure 5.5b, and Table 5.3), whereas αS56/69 has distances of 3.0 nm and 3.7 nm (Figure 5.5a, and Table 5.3). For αS56/90 and αS69/90 (Table 5.3), similar distances are found, however the width of the distance distribution of αS56/90 in the present study is larger than the one in (22) (see Figure 5.5a and b). Because of the large differences in DEER results for αS56/69 and αS56/90, we conclude that not only the morphology (chapter 4) of the fibrils differs, but also the protein fold is different for the two forms.

Next, we compare our distances with the distances reported by Pornsuwan *et al*. (21). They reported seven DEER distances. Only one pair has spin labels at positions similar to the ones measured in the present study. This is αS54/90 in (21) and αS56/90 in the present case. Pornsuwan *et al*. (21) reported the distance of 2.35 nm for αS54/90, whereas αS56/90 in the present study has the distance of

3.5 nm. The difference of 1.0 nm is large considering that 54 and 56 are only two residues apart in the sequence, and would point in the same direction of the strand, if they were on the same strand. The difference in distance of the pair αS56/90 and αS54/90 suggests that the protein folds are different. To be sure, an atomic resolution model for the fold derived from our study or (21) is needed, because against such a model, all measured distances can be compared.

5.4.3 Comparison with recently published structural models

Three structural models were published recently: a. An NMR study yielding atomic coordinates for full-length αS, which we refer to as the Rienstra model (25), b. A model based on shorter αS-fragments that form fibrils and were crystallized, which we refer to as the Eisenberg model (24), and c. a molecular dynamics (MD) simulation study of fibrils (23). We compare our data to the first two models. We used the published coordinates and modeled the spin-label linker using the MMM program (37).

5.4.3.1 Comparison with the Rienstra model (25) for the αS fibril fold

The Rienstra model (25) describes the structure of αS fibrils at atomic-resolution level. Using distance constraints derived from solid-state NMR, atomic coordinates of the αS fibril fold (pdb file: 2N0A (25)) are given. For this structure we calculated the spin-label linker conformations with MMM (37), as described in the Results section.

Overall the MMM distances derived from the ss-NMR study do not agree well with the measured ones. This is most obvious for αS56/69, αS56/75, αS56/90, αS69/85, and αS75/85. For none of these positions the experimentally

determined distances agree with those predicted from the structure. For αS69/90, the short distance predicted is just in the range where cw-EPR line broadening is small and DEER is not sensitive (38), so it could be compatible with the experimental observation. For αS42/85, the majority of the MMM predicted distance range is outside the experimental one, and only for αS42/69 and αS42/75, the MMM distances fall within one of the two distance peaks observed experimentally. For the latter two mutants, the respective distance distributions could be compatible, if one would assume that the second peak is due to an intermolecular distance.

In view of the overall disagreement, it seems possible that ss-NMR probes a different fibril fold than the present study. A different fold could be explained by the different fibrillization conditions used in (25), and be compatible with differences in the fibril morphology described in (25). To be sure, further experiments would be needed, such as a more detailed EM study on the fibrils of the present study.

5.4.3.2 Comparison with the Eisenberg model (24)

The Eisenberg model (24) describes the structure of the toxic core (called the NACore) of αS at atomic-resolution level, derived from micro-electron diffraction. This model (24) represents the αS fibril fold for residues 42 to 83 generated from the shorter fragments crystallized. We use MMM to derive distance distributions and compare with the distances from the present study (see Table 5.4)

Table 5.4. Comparison of distances from the present study with the distances derived from the model described in (24) using MMM.

mutants	distances (nm) in the present study		distances (nm)[a]	agreement
	peak 1	peak 2		
αS42/69	3.4	4.6	4.3	yes
αS42/75	3.3	4.3	3.2	yes
αS56/69	3.0	3.7	1.2	no
αS56/75	3.5	na	2.1	no

a: distances obtained from the Eisenberg model (24) using MMM

Because the Eisenberg model comprises only residues from 42 to 83, only four of our DEER distances (Table 5.4) can be compared to the model.

For αS42/69, one of the two distance peaks, the one at 4.6 nm (Figure 5.4c) is in agreement with the distance of 4.3 nm derived from the Eisenberg model by MMM. A similar situation occurs for αS42/75, where one of the two distances, 3.2 nm agrees with the distance from the Eisenberg model. The distances from the other two doubly labelled αS (αS56/69 and αS56/75) do not agree with the ones from the Eisenberg model. Therefore, we consider our distances not compatible with the Eisenberg model (24). The reason may lie in the fact that the model by Eisenberg is generated from fibrils of short fragments of αS. Long range interactions of αS may not be well-represented in that model.

In this study, we show that long–range distance constraints for the αS fibril fold can be obtained under conditions that promote fibrils of single morphology. We

show that the present results are not compatible with the recently published structural models for the αS fibril fold (24,25) in certain aspects. Whether this is due to the limitations of the present study or really reflects a difference in the fibril fold remains to be determined. Several approaches for developing DEER data of fibrils into a model for the fibril fold are possible (22,26) and we will pursue them in the future.

5.5 References

1. Parkinson J. An Essay on the Shaking Palsy (Whitingham and Rowland, London). 1817.

2. Junn E, Ronchetti RD, Quezado MM, Kim S-Y, Mouradian MM. Tissue transglutaminase-induced aggregation of α-Synuclein: Implications for Lewy body formation in Parkinson's disease and dementia with Lewy bodies. Proc Natl Acad Sci U S A. 2003;100:2047–2052.

3. Chung KK, Zhang Y, Lim KL, Tanaka Y, Huang H, Gao J, Ross CA, Dawson VL, Dawson TM. Parkin ubiquitinates the α-Synuclein-interacting protein, synphilin-1: Implications for Lewy-body formation in Parkinson disease. Nat Med. 2001;7:1144–1150.

4. Spillantini MG, Schmidt ML, Lee VM, Trojanowski JQ, Jakes R, Goedert M. α-Synuclein in Lewy bodies. Nature. 1997;388:839–840.

5. Spillantini MG, Crowther RA, Jakes R, Hasegawa M, Goedert M. α-Synuclein in filamentous inclusions of Lewy bodies from Parkinson's disease and dementia with Lewy bodies. Proc Natl Acad Sci U S A. 1998;95:6469–6473.

6. Dunker AK, Lawson JD, Brown CJ, Williams RM, Romero P, Oh JS, Oldfield CJ, Campen AM, Ratliff CM, Hipps KW, Ausio J, Nissen MS, Reeves R, Kang C, Kissinger CR, Bailey RW, Griswold MD, Chiu W, Garner EC, Obradovic Z. Intrinsically disordered protein. J Mol Graph Model. 2001;19:26–59.

7. Dyson HJ, Wright PE. Intrinsically unstructured proteins and their functions. Nat Rev Mol Cell Biol. 2005;6:197–208.

8. Fändrich M. On the structural definition of amyloid fibrils and other polypeptide aggregates. Cell Mol Life Sci. 2007;64:2066–2078.

9. Margittai M, Langen R. Fibrils with parallel in-register structure constitute a major class of amyloid fibrils: Molecular insights from electron paramagnetic resonance spectroscopy. Q Rev Biophys. 2008;41:265-297.

10. Heise H, Hoyer W, Becker S, Andronesi OC, Riedel D, Baldus M. Molecular-level secondary structure, polymorphism, and dynamics of full-length α-Synuclein fibrils studied by solid-state NMR. Proc Natl Acad Sci U S A. 2005;102:15871-15876.

11. Der-Sarkissiant A, Jao CC, Chen J, Langen R. Structural organization of α-Synuclein fibrils studied by site-directed spin labeling. J Biol Chem. 2003;278:37530–37535.

12. Chen M, Margittai M, Chen J, Langen R. Investigation of α-Synuclein fibril structure by site-directed spin labeling. J Biol Chem. 2007;282:24970–24979.

13. Heise H, Celej MS, Becker S, Riedel D, Pelah A, Kumar A, Jovin TM, Baldus M. Solid-state NMR reveals structural differences between fibrils of wild-type and disease-related A53T mutant α-Synuclein. J Mol Biol. 2008;380:444–450.

14. Bousset L, Pieri L, Ruiz-Arlandis G, Gath J, Jensen PH, Habenstein B, Madiona K, Olieric V, Bockmann A, Meier BH, Melki R. Structural and functional characterization of two α-Synuclein strains. Nat Commun. 2013;4:1-13.

15. Fändrich M, Meinhardt J, Grigorieff N. Structural polymorphism of Alzheimer Abeta and other amyloid fibrils. Prion. 2009;3:89–93.

16. Vilar M, Chou H, Lührs T, Maji SK, Riek-Loher D, Verel R, Manning G, Stahlberg H, Riek R. The fold of α-Synuclein fibrils. Proc Natl Acad Sci U S A. 2008;105:8637–8642.

17. Karyagina I, Becker S, Giller K, Riedel D, Jovin TM, Griesinger C, Bennati M. Electron paramagnetic resonance spectroscopy measures the distance between the external β-strands of folded α-Synuclein in amyloid fibrils. Biophys J. 2011;101:L1–L3.

18. Hashemi Shabestari M, Segers-Nolten IMJ, Claessens MMAE, van Rooijen BD, Subramaniam V, Huber M. Elucidating the α-Synuclein fibril fold by pulsed EPR. Biophys J. 2012;102:454a.

19. Gath J, Habenstein B, Bousset L, Melki R, Meier BH, Böckmann A. Solid-state NMR sequential assignments of α-Synuclein. Biomol NMR Assign. 2012;6:51–55.

20. Comellas G, Lemkau LR, Zhou DH, George JM, Rienstra CM. Structural intermediates during α-Synuclein fibrillogenesis on phospholipid vesicles. J Am Chem Soc. 2012;134:5090–5099.

21. Pornsuwan S, Giller K, Riedel D, Becker S, Griesinger C, Bennati M. Long-range

distances in amyloid fibrils of α-Synuclein from PELDOR spectroscopy. Angew Chemie-Int Ed. 2013;52:10290–10294.

22. Hashemi Shabestari M, Kumar P, Segers-Nolten IMJ, Claessens MMAE, van Rooijen BD, Subramaniam V, Huber M. Three long-range distance constraints and an approach towards a model for the α-Synuclein-fibril fold. Appl Magn Reson. 2015;46:369–388.

23. Atsmon-Raz Y, Miller Y. A proposed atomic structure of the self-assembly of the non-amyloid-β component of human α-Synuclein as derived by computational tools. J Phys Chem B. 2015;119:10005–10015.

24. Rodriguez JA, Ivanova MI, Sawaya MR, Cascio D, Reyes FE, Shi D, Sangwan S, Guenther EL, Johnson LM, Zhang M, Jiang L, Arbing MA, Nannenga BL, Hattne J, Whittelegge J, Brewster AS, Messerschmidt M, Boutet S, Sauter NK, Gonen T, Eisenberg DS. Structure of the toxic core of α-Synuclein from invisible crystals. Nature. 2015;525:486–490.

25. Tuttle MD, Comellas G, Nieuwkoop AJ, Covell DJ, Berthold DA, Kloepper KD, courtney JM, Kim JK, Barclay AM, Kendall A, Wan W, Stubbs G, Schwieters CD, Lee VM, Goerge JM, Rienstra CM. Solid-state NMR structure of a pathogenic fibril of full-length human α-Synuclein. Nat Struct Mol Biol. 2016;23:409–415.

26. Bedrood S, Li Y, Isas JM, Hegde BG, Baxa U, Haworth IS, Langen R. Fibril structure of human islet amyloid polypeptide. J Biol Chem. 2012;287:5235–5241.

27. Jeschke G. Distance measurements in the nanometer range by pulse EPR. ChemPhysChem. 2002;3:927–932.

28. Jeschke G. Determination of the Nanostructure of Polymer Materials by Electron Paramagnetic Resonance Spectroscopy. Macromol Rapid Commun. 2002;23:227–246.

29. Jeschke G, Koch A, Jonas U, Godt A. Direct conversion of EPR dipolar time evolution data to distance distributions. J Magn Reson. 2002;155:72–82.

30. Jeschke G, Polyhach Y. Distance measurements on spin-labelled biomacromolecules by pulsed electron paramagnetic resonance. Phys Chem Chem Phys. 2007;9:1895-1910.

31. Sidhu A, Segers-Nolten I, Subramaniam V. Solution conditions define morphological homogeneity of α-Synuclein fibrils. Biochim Biophys Acta. 2014;1844:2127–2134.

32. van Raaij ME, Segers-Nolten IMJ, Subramaniam V. Quantitative morphological analysis reveals ultrastructural diversity of amyloid fibrils from α-Synuclein

mutants. Biophys J. 2006;91:L96–L98.

33. Veldhuis G, Segers-Nolten I, Ferlemann E, Subramaniam V. Single-molecule FRET reveals structural heterogeneity of SDS-bound α-Synuclein. ChemBioChem. 2009;10:436–439.

34. Drescher M, Godschalk F, Veldhuis G, van Rooijen BD, Subramaniam V, Huber M. Spin-label EPR on α-Synuclein reveals differences in the membrane binding affinity of the two antiparallel helices. ChemBioChem. 2008;9:2411–2416.

35. Drescher M, Veldhuis G, Van Rooijen BD, Milikisyants S, Subramaniam V, Huber M. Antiparallel arrangement of the helices of vesicle-bound α-Synuclein. J Am Chem Soc. 2008;130:7796–7797.

36. Jeschke G, Chechik V, Ionita P, Godt A, Zimmermann H, Banham J, Timmel CR, Hilger D, Jung H. DeerAnalysis2006 - a comprehensive software package for analyzing pulsed ELDOR data. Appl Magn Reson. 2006;30:473–498.

37. Polyhach Y, Bordignon E, Jeschke G. Rotamer libraries of spin labelled cysteines for protein studies. Phys Chem Chem Phys. 2011;13:2356–2366.

38. Banham JE, Baker CM, Ceola S, Day IJ, Grant GH, Groenen EJJ, Rodgers CT, Jeschke G, Timmel CR. Distance measurements in the borderline region of applicability of CW EPR and DEER: A model study on a homologous series of spin-labelled peptides. J Magn Reson. 2008;191:202–218.

Appendix C to chapter 5

The DEER method is not sensitive to short distances, which under the conditions of the experiments in chapter 5, applies to distances below 2 nm. Therefore, it is customary to complement DEER experiments with low temperature cw-EPR, as the latter method reveals short distances between spins, i.e., distances below 2 nm by spectral line broadening. To detect this broadening, reference spectra are needed that give the lineshape in the absence of spin-spin interaction. For the samples investigated here, the reference spectra are the spectra of 1:1 mixture of spectra of the respective singly labelled αS-fibril-reference spectra. Spectra of some of the fibrillized singly spin-labeled αS show broadening with respect to a spectrum of a spin label in frozen solution at the same concentration. This concerns the spectra of αS42, αS56, αS69, and αS75, whereas αS85 and αS90 are not broadened. We attribute this broadening to intermolecular interactions, and note that it is intriguing that some positions show this broadening and others do not.

To determine whether short intramolecular distances occur in the fibrils of the doubly-labelled αS protein, the broadening of the reference spectra is a complication.

Figure C1 shows the EPR spectra of doubly labelled αS superimposed on the spectra of the 1:1 mixture of the respective reference spectra (for details, see Figure caption). The lineshapes of the spectra of αS42/69, αS42/75, αS42/85, αS56/69, and αS75/85, are close to those of their respective references, showing the absence of short intramolecular distances, while the lineshapes of the spectra of αS56/75, αS56/90, and αS69/85 are broader than their reference spectra.

To test the influence of the reference spectra on this result, in Figure C2, the spectra that show broadening in Figure C1 are compared to the most broadened

cw-EPR spectra of the respective singly-labelled αS. In the comparison in Figure C2, αS69/85 is not broadened, showing that the composition of the reference spectra has a strong effect on the outcome and suggesting that the broadening of αS69/85 has an intermolecular component. The double mutants αS56/75, and αS56/90 show broadening in Figure C2, which could be intramolecular. It corresponds to a distance in the order of 2 nm for two-spin interaction. Because the lineshape of the reference spectra depends on the ratio by which the spectra of the two singly labelled αS fibrils are added, the reference lineshape is uncertain. Therefore, a clear assignment to inter or intramolecular distances is not possible, and the cw-EPR data for αS56/75 and αS56/90 are not conclusive. Given the DEER data, it is more likely that the broadening is due to intermolecular interactions.

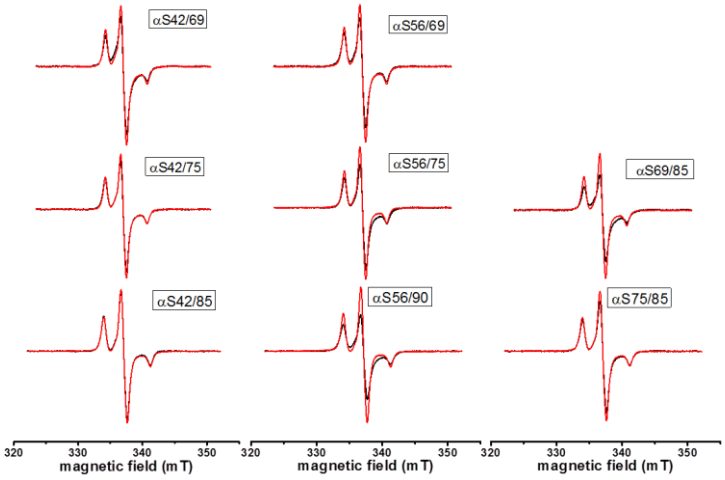

Figure C1. Continuous-wave EPR spectra of the fibrils in frozen solution of all the doubly labelled αS proteins (black) superimposed with the 1:1 mixture of spectra of the respective singly labelled counterparts (red). Field scale applies to all vertically displaced spectra.

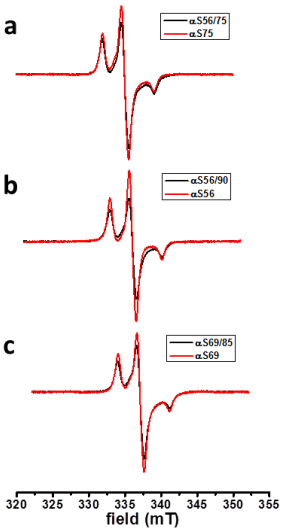

Figure C2. Comparison of the spectra of doubly labelled αS fibrils in frozen solution superimposed with spectra of the respective singly labelled variants showing most broadened lineshape; a. the spectrum of αS56/75 (black) with that of αS75 (red), b. the spectrum of αS56/90 (black) with that of αS56 (red), and c. the spectrum of αS69/85 (black) with that of αS69 (red).

Appendix D to chapter 5: Exploring Methods to Increase the DEER Evolution Time in α-Synuclein Fibrils: Deuteration of Buffer and 35 GHz DEER

Longer DEER evolution times improve the sensitivity for longer distances. For α-Synuclein (αS) fibrils, we tested two commonly used approaches: replacing protons by deuterons to increase the T_2 time of the electron spin and DEER at 35 GHz to make use of the higher sensitivity. Both approaches were tested on the αS56/69 mutant in preparation of the experiments described in chapter 4 and 5.

Materials and methods

Expression and purification of cysteine mutants of the αS were performed as described in chapter 5.

Preparation and harvesting of fibrillar αS

Fibrils of αS were formed by incubating monomer solutions at a total protein concentration of 100 µM. Fibrils of the doubly spin-labelled mutant were prepared with a diamagnetic dilution of 1 in 20, using 5 µM spin-labeled αS with 95 µM wild-type protein. The fibrils of the corresponding singly labeled mutants were prepared using a diamagnetic dilution of 10 µM spin-labeled αS in the presence of 90 µM wild-type αS (1 in 10), to keep the spin-label concentrations constant. All aggregations were performed in 10 mM Tris – HCl, 50 mM NaCl, pH 7.4 buffer (abbreviated as H_2O-Tris buffer). The total volume of the mixture was 3.0 ml, which was aliquoted into three Eppendorf tubes (Eppendorf LoProtein Bind 2ml), 1.0 ml each. All tubes were incubated at a temperature of 37 ^{o}C with constant shaking at 1000 rpm in a Thermo mixer (Eppendorf). The time evolution of αS aggregation was monitored by the standard Thioflavin T (ThioT)

fluorescence assay. For each tube, fibrillization was stopped when the ThioT-fluorescence intensity reached a plateau. The fibrillization was generally completed in 6-8 days. Fibrils were harvested by ultra- centrifugation for 30 min at 120000xg using 70.1Ti rotor in a Beckman Coulter Ultracentrifuge. Centrifugation was performed at 4^{o}C. The fibril pellets were washed three times by resuspending the pellets each time in 2.5 ml buffer used for fibrillization and re-centrifuging as described above. Glycerol (20 % (v/v)) was added to the washed fibril pellets before transferring them into the 3 mm (outer diameter) quartz tubes. The sample tubes were plunged into liquid nitrogen for fast freezing. These samples were used for EPR measurements.

Fibrils with deuterated buffer were prepared the same way as described above, however, the washing steps were done by resuspending into deuterated Tris-HCl (D_2O-Tris), pH 7.4 buffer three times and re-centrifuging as described above. The buffer has the same composition as used for aggregation, but was prepared by dissolving the buffer salts in D_2O instead of H_2O. After the final wash, 20 % (v/v) of deuterated glycerol (glycerol-d_8) was added to the fibril pellet. The fibril pellet was transferred into the EPR tube and flash-frozen in liquid N_2. We tested this approach with one set of spin-labeled αS mutants (αS56/69, αS56 and αS69).

T2 echo decay experiment

The two-pulse echo decay experiments were performed at 9.5 GHz on an ELEXSYS E680 spectrometer (Bruker, Rheinstetten, Germany) using a 3 mm split-ring resonator (ER 4118XMS-3-W1). The temperature was kept at 40 K with a helium-gas stream using a CF935 (Oxford Instruments, United Kingdom) cryostat with an ITC502 temperature controller (Oxford Instruments, United Kingdom). The pulse lengths for the two pulses, π/2- and π-pulses, were 80 and 160 ns. The initial separation of the two pulses was 120 ns.

DEER measurements

The DEER measurements were performed at 9.5 GHz and 35 GHz. The DEER measurements at 9.5 GHz were performed on an ELEXSYS E680 spectrometer (Bruker, Rheinstetten, Germany) using a 3 mm split-ring resonator (ER 4118XMS-3-W1). The temperature was kept at 40 K with a helium-gas stream using a CF935 (Oxford Instruments, United Kingdom) cryostat with an ITC502 temperature controller (Oxford Instruments, United Kingdom). The pump and observer frequencies were separated by 70 MHz and adjusted as reported before (1). The pump-pulse power was adjusted to invert the echo maximally (2). The pump-pulse length was set to 16 ns. The pulse lengths of the observer channel were 16 and 32 ns for π/2- and π - pulses, respectively. All DEER measurements were performed as two-dimensional experiments, to suppress the proton modulation. To do so, DEER time traces were measured for ten different τ -values spaced by 8 ns starting at τ = 200 ns. The typical accumulation times per sample were 16 h.

The 35 GHz DEER experiments were performed on the samples used for 9.5 GHz DEER. An ELEXSYS E580 spectrometer (Bruker, Rheinstetten, Germany) with a 3 mm, 35 GHz EPR resonator with a 150 W TWT amplifier was used. Temperature: 33 resp. 45 K; separation of pump and observer frequencies of 64.4 MHz. The pump-pulse was adjusted to the maximum of the echo-detected field-sweep spectrum and the observer-frequency to a frequency corresponding to 2.2 mT higher field. The pump-pulse lengths were optimized to maximally invert the echo and were between 14 and 20 ns. The pulse lengths of the observer channel were 10 and 20 ns for π/2- and π - pulses, respectively. The complete pulse sequence is given by: $\frac{\pi}{2_{\mathrm{obs}}} - \tau_1 - \pi_{\mathrm{obs}} - t - \pi_{\mathrm{pump}} - (\tau_1 + \tau_2 - t) - \pi_{\mathrm{obs}} - \tau_2 - \mathrm{echo}$. The DEER time traces for ten different τ_1 values spaced by 8 ns, starting at τ_1 = 180 ns were added to suppress nuclear modulations. Accumulation time per sample was

2 hours. These experiments were performed at Bruker, Biospin Rheinstetten, Germany and we thank Patrick Carl for making this possible.

Results and discussion

Comparison of fibrils in deuterated and protonated buffer

To see the effect of D_2O exchange on the T_2 relaxation time for the αS56/69 fibril samples, we performed a two-pulse echo-decay experiment. The echo-decay times of αS56/69 fibrils in deuterated or protonated buffer are the same (Figure D1). At the first sight this result is surprising. Deuterating the buffer of soluble spin labelled proteins results in longer T_2 times, because protons are more effective than deuterons in enhancing T_2 relaxation of electron spins (3). Apparently, the high proton content of the fibril itself is sufficient to cause T_2 relaxation in the fibril samples, whether the buffer is deuterated or not. Therefore, the experiments described in chapter 4 and 5 were performed using protonated buffer. By harvesting the fibrils more efficiently, we were successful to extend the evolution times from 1.5 µs in previous experiments to an evolution time of 1.8 µs.

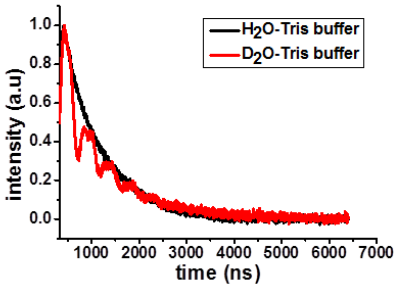

Figure D1. Effect of D_2O exchange on the T_2 relaxation time for the αS56/69 fibril sample; T_2 echo decay of αS56/69 fibril with H_2O-tris buffer (black) and D_2O-tris buffer (red).

Comparison of DEER measurements of αS56/69 fibrils at 9.5 GHz and 35 GHz

With 35 GHz DEER, a longer evolution time of 2.2 µs and also a better signal to noise ratio is obtained than at 9.5 GHz. In Figure D2, the DEER data are shown. The distance distributions obtained after Tikhonov regularization show that both distributions have the most intense peak around 2.5 nm. In the DEER trace obtained at 35 GHz, this peak is more pronounced and shifted to shorter distances, which we attribute to a better separation of background and modulation, which is the result of the longer evolution time at 35 GHz. These results show that also for fibril samples, DEER at 35 GHz is advantageous.

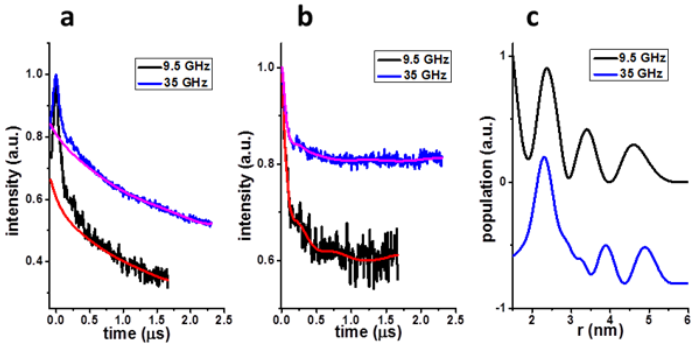

Figure D2. Results of DEER experiments for αS56/69 fibril samples at 9.5 GHz (black line) and 35 GHz (blue line): a. DEER time traces with experimental background, b. DEER time traces after background correction along with the fits corresponding to the distance distributions shown in c; c. distance distributions derived from DEER data after Tikhonov regularization with a regularization parameter α of 100. DEER time traces are normalized (maximum echo intensity is set to one) and shifted vertically for better visibility.

References

1. Drescher M, Veldhuis G, van Rooijen BD, Milikisyants S, Subramaniam V, Huber M. Antiparallel arrangement of the helices of vesicle-bound α-Synuclein. J Am Chem Soc. 2008;130:7796–7797.

2. Jeschke G. Distance measurements in the nanometer range by pulse EPR. ChemPhysChem. 2002;3:927–932.

3. Huber M, Lindgren M, Hammarström P, Mårtensson LG, Carlsson U, Eaton GR, Eaton SS. Phase memory relaxation times of spin labels in human carbonic anhydrase II: Pulsed EPR to determine spin label location. Biophys Chem. 2001;94:245–256.